Characteristics of clustered heavy precipitation events at Northeast China and associated atmospheric circulations

Shunli Jiang[1] · Tingting Han[1,2,3] · Botao Zhou[1,2] · Qiushi Zhang[4] · Xin Hao[1,2,3] · Huixin Li[1,2,3]

Abstract

Heavy precipitation events can exert greater impact than general precipitation on the economy, ecology, and people's livelihoods. Based on CN05.1 daily precipitation data and the NCEP/NCAR global daily reanalysis dataset, this study analyzes the characteristics of clustered heavy precipitation (CHP) events during summer in Northeast China (NEC) during 1961–2020, with consideration of associated atmospheric circulations and moisture transport. Results indicate that CHP events occurred mainly during midsummer, especially in July. Both the frequency and the intensity of CHP events decrease after the mid-1970s, increase after the early 1980s, and then diminish again after the 2000s. The CHP events occur in association with an anomalous lower-tropospheric cyclone centered over NEC, northward and westward shifts of the western North Pacific subtropical high in the middle troposphere, and northward shift of an intensified westerly jet in the upper troposphere, in conjunction with strengthened local convective motion. Additionally, the net moisture budget begins to increase 2 days before the occurrence of CHP and peaks 6 h earlier than the CHP. Further results indicate that net moisture influx across the southern boundary of NEC made a dominant contribution to the net moisture budget. The results of this study have importance regarding the prediction of CHP events over NEC.

1 Introduction

Northeast China (NEC), with its vast area of arable land, is an important commodity grain production base. Under the background of global warming, both precipitation and heavy precipitation have increased during recent years (Xu et al. 2011; Sun and Ao 2013; IPCC 2021). Anomalous variations in precipitation in NEC might lead to increased instability in grain production (Du et al. 2013). Moreover, heavy precipitation events can cause erosion, landslides, debris flows (Ban et al. 2015), and floods (Cao et al. 2018; Breugem et al. 2020). In comparison with general heavy precipitation, clustered heavy precipitation (CHP) can result in disasters of greater magnitude (Li et al. 2016). Therefore, it is essential to understand the rules that govern CHP events in NEC during summer.

Summer is the main season of precipitation in NEC (Gong et al. 2006; Liang et al. 2011; Gao and Gao 2018). Previous studies have revealed the spatial characteristics of summer precipitation over NEC, i.e., reduction in total precipitation amount from the southeast to the northwest (Wu et al. 2021; Xu and Li 2021; Yu and Ma 2022). Additionally, summer precipitation over NEC exhibits spatial heterogeneity and regional diversity (Gong et al. 2006; Yao et al. 2010; Song et al. 2015). Some studies have suggested that the systems that affect precipitation over NEC are different during the summer months (Zhao et al. 2018; Breugem et al. 2020). Precipitation over NEC during early summer (June) is affected by the activities of the Northeast China cold

✉ Tingting Han
hantt08@126.com

1 School of Atmospheric Sciences, Nanjing University of Information Science and Technology, Nanjing, China

2 Collaborative Innovation Center on Forecast and Evaluation of Meteorological Disasters/Key Laboratory of Meteorological Disaster, Ministry of Education, Nanjing University for Information Science and Technology, Nanjing, China

3 Nansen-Zhu International Research Centre, Institute of Atmospheric Physics, Chinese Academy of Sciences, Beijing, China

4 Heilongjiang Sub-Bureau of Northeast Air Traffic Management Bureau, Ha'erbin, China

vortex (Lin et al. 2021), whereas midsummer precipitation (July–August) is mainly influenced by the western North Pacific subtropical high (WNPSH) and by the mid-latitude westerly belt system (Shen et al. 2011). Meng et al. (2022) indicated that eastern and central Pacific El Niño events are followed by different precipitation anomaly patterns in the following summers. Also, summer precipitation over NEC shows interdecadal variation (Gao et al. 2014; Li 2019). Specifically, precipitation over NEC has reduced since the mid-1960s, increased after the early 1980s, and diminished remarkably since the late 1990s (Ding and Chen 2015; Han et al. 2015). During 1983–1997, the regimes associate with NEC precipitation comprised a zonal tripole pattern in the mid–high latitudes of the North Asia–Pacific region and an anomalous anticyclone centered over Japan (Han et al. 2017). After the late 1990s, summer precipitation over NEC is influenced mainly by a zonal dipole pattern (Huang et al. 2013) and an anomalous anticyclone elongated from NEC to Mongolia (Xu et al. 2015).

With increasing occurrences of extreme weather events during recent years, some research efforts have been devoted to investigating the changes in heavy precipitation and in associated atmospheric circulations (e.g., Du et al. 2013; Cao et al. 2018). Previous studies reported that heavy precipitation is the greatest contributor to total precipitation in NEC (Song et al. 2015; Wang et al. 2013), and that the contribution rate exhibits insignificant trend during 1961–2013 (Fang et al. 2017). Wu et al. (2019) documented that short-term heavy precipitation events are limited in spatial scale, and that long-term events cover a wide area. Heavy precipitation events can be influenced by the East Asian summer monsoon (Wang et al. 2017), meridional shift of the WNPSH (Gao et al. 2014), meridional position and intensity of the upper-level westerlies over East Asia (Cao et al. 2018), cut-off lows (Zhao and Sun 2006; Hu et al. 2010), and East Asian trough (Wang and He 2015). In addition, the topographic uplift affects heavy precipitation by the modulation of vertical movement (Zhang et al. 2022). The eastern and southern NEC are vulnerable to heavy precipitation events (Du et al. 2013; Wang et al. 2019; Xu and Li 2021). From the above discussion, previous studies mainly focus on spatiotemporal changes of heavy precipitation over NEC, and atmospheric circulation anomalies related to one certain event, whereas few refer to the characteristics of multiple clustered heavy precipitation cases during the past six decades and associated atmospheric regimes, which is the central issue of this study.

It is well acknowledged that water vapor transport (WVT) is of great importance for precipitation (Chen et al. 2012a; Gimeno et al. 2012; Sun et al. 2011; Li et al. 2016; Hu et al. 2018). Additionally, precipitation anomalies are highly connected with anomalous WVT (Zhou and Yu 2005; Huang et al. 2015; Gimeno et al. 2016). The WVT budget is obviously reduced in association with the diminished precipitation over NEC after the late 1990s (Han et al. 2015). The intensity of WVT related to heavy precipitation events is stronger than that associated with general precipitation (Li et al. 2016). Li et al. (2019) identified that the difference in WVT between heavy precipitation and ordinary precipitation over NEC is related to meridional WVT. However, the WVT anomalies across each boundary associated with the CHP events, especially the WVT anomalies leading the occurrence of CHP, remains unclear, which is an issue of this study.

The remainder of this paper is structured as follows. Section 2 introduces the datasets and methods used in the study. Section 3 describes the interannual and interdecadal characteristics of CHP events during summer over NEC and discusses the associated atmospheric circulations and moisture transport. Finally, a brief summary of the main findings is presented in Sect. 4.

2 Data and methods

This study uses an advanced high-resolution ($0.25° \times 0.25°$) daily rainfall observation dataset (i.e., CN05.1) (Wu and Gao 2013), which is constructed based on interpolation of data from more than 2400 meteorological stations in China. Daily and 6-hourly mean reanalysis data for 1961–2020, with horizontal resolution of $2.5° \times 2.5°$, are obtained from the National Centers for Environmental Prediction/National Center for Atmospheric Research (NCEP/NCAR) (Kalnay et al. 1996). The study area comprised NEC, which is defined as the region within 38°–54° N, 115°–135° E.

Composite and correlation analyses are used to analyze the circulation and WVT related to CHP events over NEC during summer. In this study, a CHP event is determined on the basis of the following two conditions: (1) daily precipitation is greater than the threshold value of heavy precipitation, and (2) more than 40% of the grid points in NEC satisfied condition (1) at the same time. The threshold value of heavy precipitation is defined as the 90th percentile value of precipitation > 0.1 mm in the daily precipitation data during 1961–2020. Summer is defined as the months of June, July, and August. Additionally, to analyze atmospheric stability, we calculate the K index as follows (Chen et al. 2012b):

$$K = \left(T_{850} - T_{500} \right) + T_{d850} - \left(T - T_d \right)_{700}$$

and we calculate the moisture flux vector Q as follows (Trenberth et al. 2007):

$$Q = Q_\lambda \vec{i} + Q_\phi \vec{j}$$

$$Q_\lambda = -\frac{1}{g}\int_{p_s}^{p_t}(qu)dp, Q_\phi = -\frac{1}{g}\int_{p_s}^{p_t}(qv)dp$$

where Q_λ is the integral of vertical WVT longitudinally, Q_ϕ is the integral of vertical WVT latitudinally, p_s is the surface pressure, p_t is 300 hPa and g is 9.80665 (m s^{-2}). The vertical integration of water vapor flux is calculated approximately according to the trapezoidal rule, and because complex terrain will affect the vertical integration of water vapor flux, this study used the method of integrating from the surface pressure to eliminate the impact of complex terrain (Li et al. 2016). In addition, we used the method in Sun et al. (2011) to calculate the moisture budget and horizontal moisture flux divergence.

3 Results

3.1 Characteristics of clustered heavy precipitation events in NEC

According to the definition in Sect. 2, 75 CHP events occur in summer over NEC during 1961–2020 (Table 1). Overall, 5 events occur during June and 70 cases appear in July–August, with more than half of those 70 cases observed in July (Fig. 1), i.e., CHP in NEC mainly occurs during mid-summer. Moreover, the numbers of CHP events during the latter 10 days of July significantly exceed those during both the first and middle 10 days of the month. In August, CHP events appear most frequently during the middle 10 days of the month, follow by the latter 10 days; the numbers of CHP events during the first 10 days of August are the lowest. Figure 2 shows the decadal characteristics of the monthly and summer-mean CHP events for the previous 60 years. Higher occurrence of CHP during summer is observed during the 1980s and 1990s than in other decades, which is consistent with the decadal variation in CHP during July. Additionally, 59 of the 75 CHP events (approximately 79%) occur before 2000, and the remaining 16 events (approximately 21%) occur after 2000. The reduction in CHP events during the 2000s is mainly attributed to reduced CHP in July, and the reduction in CHP events during 2011–2020 is attributed to reduction in CHP during June and August (Fig. 2a).

Figure 3 illustrates the temporal evolutions of the frequency/intensity of summer CHP events, and the CHP amounts over NEC during 1961–2020. In-phase variations are observed in the time series of frequency/intensity/amounts of CHP events during the past six decades. Specifically, they all have decreased around the mid-1970s, increased after the 1980s, and then reduced since the late 1990s (Fig. 3d). Moreover, the averages of CHP intensity and amounts are 11.30 mm per day and 20.27 mm per year, separately. The maximum of the CHP intensity is 24.66 mm

Table 1 The 75 CHP events over NEC during 1961–2020

Year	Month	Day	Year	Month	Day
1961	Jul	12	1989	Jul	18
1962	Jul	10	1989	Jul	23
1962	Jul	17	1990	Jul	7
1962	Jul	26	1990	Jul	8
1963	Jul	15	1990	Aug	28
1963	Jul	28	1991	Jul	22
1965	Aug	3	1991	Jul	29
1966	Jul	29	1991	Jul	30
1967	Jul	19	1992	Jul	26
1968	Aug	17	1993	Aug	24
1969	Aug	12	1994	Jul	9
1969	Aug	17	1994	Jul	13
1969	Aug	18	1994	Aug	6
1969	Aug	22	1996	Jul	29
1971	Jul	26	1996	Aug	2
1971	Jul	27	1997	Aug	1
1972	Jul	20	1997	Aug	21
1972	Jul	21	1998	Jul	6
1973	Jul	20	1998	Jul	7
1973	Aug	21	1998	Aug	11
1974	Aug	1	2000	Jul	20
1976	Jul	29	2002	Jun	10
1977	Jul	3	2003	Jul	27
1977	Jul	24	2003	Aug	22
1977	Jul	29	2004	Aug	3
1981	Jun	21	2004	Aug	28
1981	Jul	4	2008	Aug	1
1981	Jul	8	2009	Jun	19
1982	Aug	17	2009	Aug	20
1983	Jul	14	2012	Jul	22
1984	Jul	12	2013	Jul	2
1984	Aug	13	2013	Jul	16
1985	Jul	22	2013	Jul	28
1985	Aug	25	2014	Jul	8
1986	Jun	28	2014	Jul	21
1987	Aug	27	2018	Jul	24
1988	Jul	8	2020	Aug	13
1989	Jun	14			

per day, occurring on 22th July, 2012. The maximum of the CHP amounts is 66.15 mm, occurring in 1969. The CHP events are highly linked with atmospheric circulations and moisture transportation anomalies, which will be explored in Sect. 3.2.

3.2 Atmospheric circulation associated with CHP

Atmospheric circulation anomaly is the most direct contributor to the occurrence of heavy precipitation events. Different
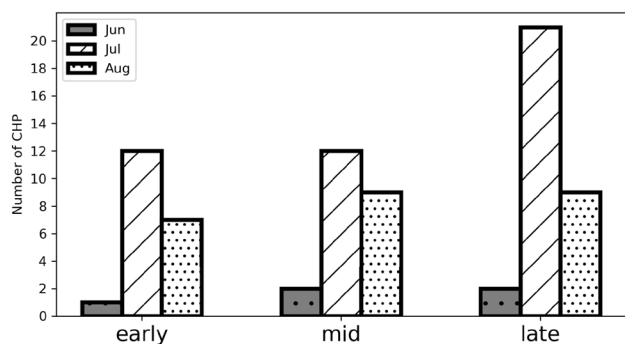
Fig. 1 Ten-day characteristics of CHP frequency (day) during summer over NEC during 1961–2020. The first, middle and latter 10 days of June refer to 1st June to 10th June, 11th June to 20th June, 21st June to 30th June, respectively. The first, middle and latter 10 days of July (August) refer to 1st July (August) to 10th July (August), 11th July (August) to 20th July (August), 21st July (August) to 31st July (August), respectively

precipitation modes are attributed to different circulation anomalies (Han et al. 2019). Therefore, atmospheric circulations associated with CHP events over NEC are explored in this section. Figure 4 shows the spatial distributions of sea level pressure anomalies, 850-hPa geopotential height/horizontal wind anomalies, 500-hPa geopotential height anomalies, and 200-hPa zonal wind anomalies associated with the studied CHP events over NEC. As shown in Fig. 4a, the CHP events occur with marked negative height anomalies over East China, with an anomalous center over NEC, and positive height anomalies over the Northwest Pacific. In the middle troposphere, anomalous positive geopotential height can be seen over the Japanese archipelago and southern China, together with negative anomalies centered over NEC (Fig. 4b, c). Previous study has suggested that an

anomalous low over NEC is favorable for enhanced local precipitation (Shen et al. 2011). Consistently, remarkable cyclonic wind anomalies are evident centered over NEC, together with anticyclonic wind anomalies centered over the Northwest Pacific. Anomalous southwesterly or southerly winds on the western flank of the anticyclone transport warm humid air from the western Pacific toward NEC across the southern boundary (Fig. 4b). When CHP events occur, the WNPSH ridge is located at approximately 33° N, which is approximately 8° further north of its summer mean position (Fig. 4c). Generally, the rain belt is often located 6°–10° north of the WNPSH ridge (Zhu 2007), which covers part of NEC. Additionally, the western point of the WNPSH ridge is located at approximately 123°E when CHP events occur over NEC, which is 10° further west of the summer mean position (Fig. 4c). Previous studies showed that northwestward shift of the WNPSH is conducive to intensified transport of moisture toward NEC (Gao and Gao 2018; Cao et al. 2018). Therefore, the westward and northward shifts of the WNPSH are favorable for the occurrence of CHP over NEC. Additionally, in the upper levels, a significant westerly anomaly is elongated over northern China and an easterly anomaly is extended from southern China to the Northwest Pacific Ocean (Fig. 4d). The position of the westerly jet axis is abnormally northward when CHP events occur over NEC. Specifically, it is generally located to the south part of NEC, whereas it is located over the middle part of NEC when CHP occurs. Cao et al. (2018) showed that northward shift of the upper-level westerlies over NEC is beneficial for the occurrence of heavy precipitation events.

Atmospheric stability is of major importance regarding the occurrence of heavy precipitation events (Li et al. 2016). The K index is a meteorological index that describes atmospheric stability (Chen et al. 2012b); the larger the K value,
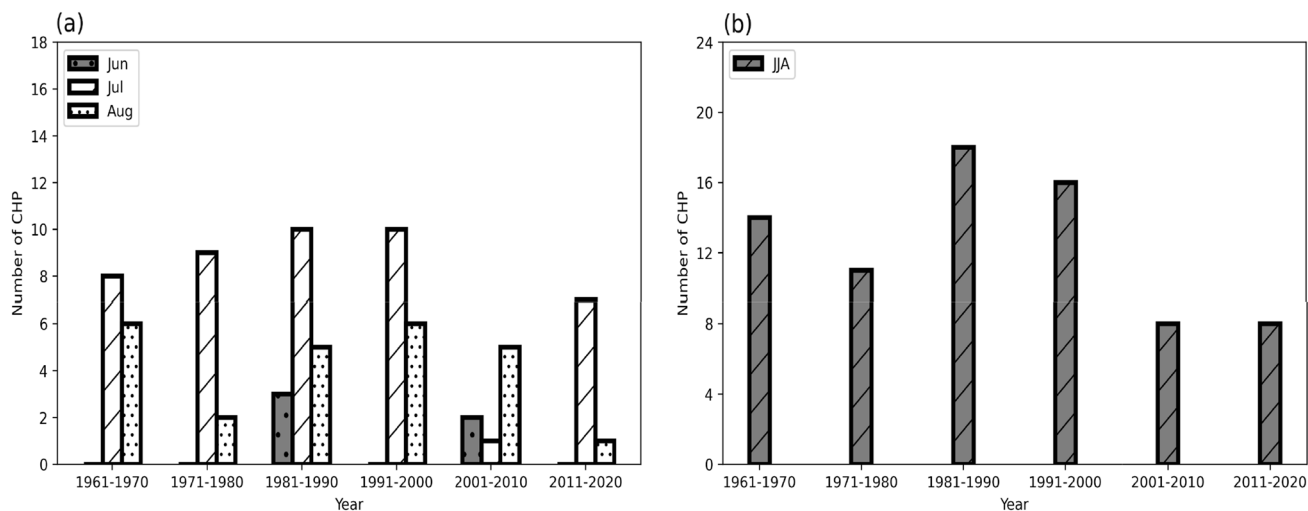
Fig. 2 Decadal variations of CHP frequency (day) over NEC during 1961–2020: **a** summer months and **b** summer mean
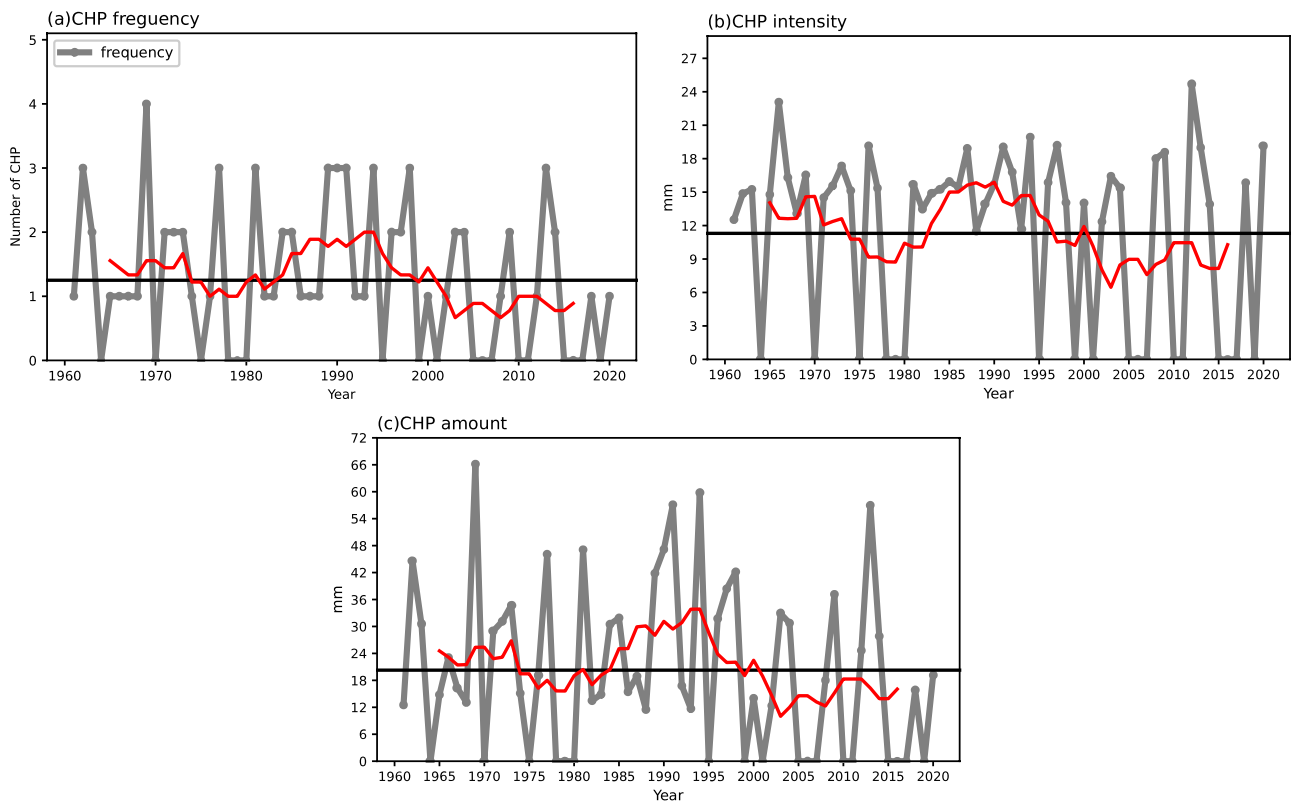
Fig. 3 Temporal evolution of **a** CHP frequency (day, gray line), **b** CHP intensity (mm day^{-1}, gray line) and **c** CHP amounts (mm year^{-1}, gray line) over NEC in summer during 1961–2020. The red line and black line represent the 9-year moving mean and the average for the past six decades, respectively

the more unstable the atmospheric circulation. Anomalies of wind divergence at lower and upper levels are shown in Fig. 5a, b, respectively, and K value anomalies at 850 and 200 hPa, as well as the vertical velocity anomalies, are shown in Fig. 5c, d, respectively. Characteristically, CHP events are associated with significant lower-layer convergence anomalies and upper-layer divergence anomalies over NEC, which excite dominant local upward movement anomalies (Fig. 5c, d). Moreover, an anomalous anticyclone is centered over southeastern parts of NEC, together with easterly anomalies over southern China and southwesterly anomalies over NEC. This is consistent with the zonal wind anomalies related to CHP (Fig. 4d). Accordingly, the K values centered on NEC increase significantly when CHP affects NEC (Fig. 5c, d). It suggests that increased unstable energy over NEC is beneficial for the occurrence of CHP.

The formation of precipitation is closely related to WVT, and abnormal WVT has important indicative significance regarding change in regional precipitation. The vertically integrated WVT during summer and the moisture anomalies for CHP events over NEC are presented in Fig. 6a, b, respectively. The moisture during summer over NEC mainly originates from the subtropical western Pacific, South China

Sea, and South Asian monsoon areas (Fig. 6a), which is consistent with the findings of Sun et al. (2007). Compared with the climatology, when CHP events occur over NEC, the southerly flow over East China strengthens markedly and transports moisture northward to NEC across the southern boundary. Accordingly, anomalous moisture convergence dominates NEC and a cyclonic moisture anomaly is centered over NEC. Additionally, an anticyclonic moisture anomaly is located over the Sea of Japan. The southwesterly flow on the western flank of the anticyclonic moisture anomaly transports water vapor from the Northwest Pacific to NEC across the southern boundary. Moreover, the anomalous westerly flow crossing the western boundary is intensified and transports water vapor from inland areas to NEC.

Figure 7 illustrates the WVT anomalies and the associated moisture divergence at different levels associated with CHP over NEC. Because atmospheric moisture lies primarily in the lower layers of the atmosphere (Sun et al. 2011; Piao et al. 2021), the WVT anomaly diminishes in the upper levels (Fig. 7c, d). The anomalous WVT associated with CHP over NEC can be tracked southward to the subtropical Northwest Pacific, and northward to inland areas near the surface (Fig. 7a). Anomalous moisture
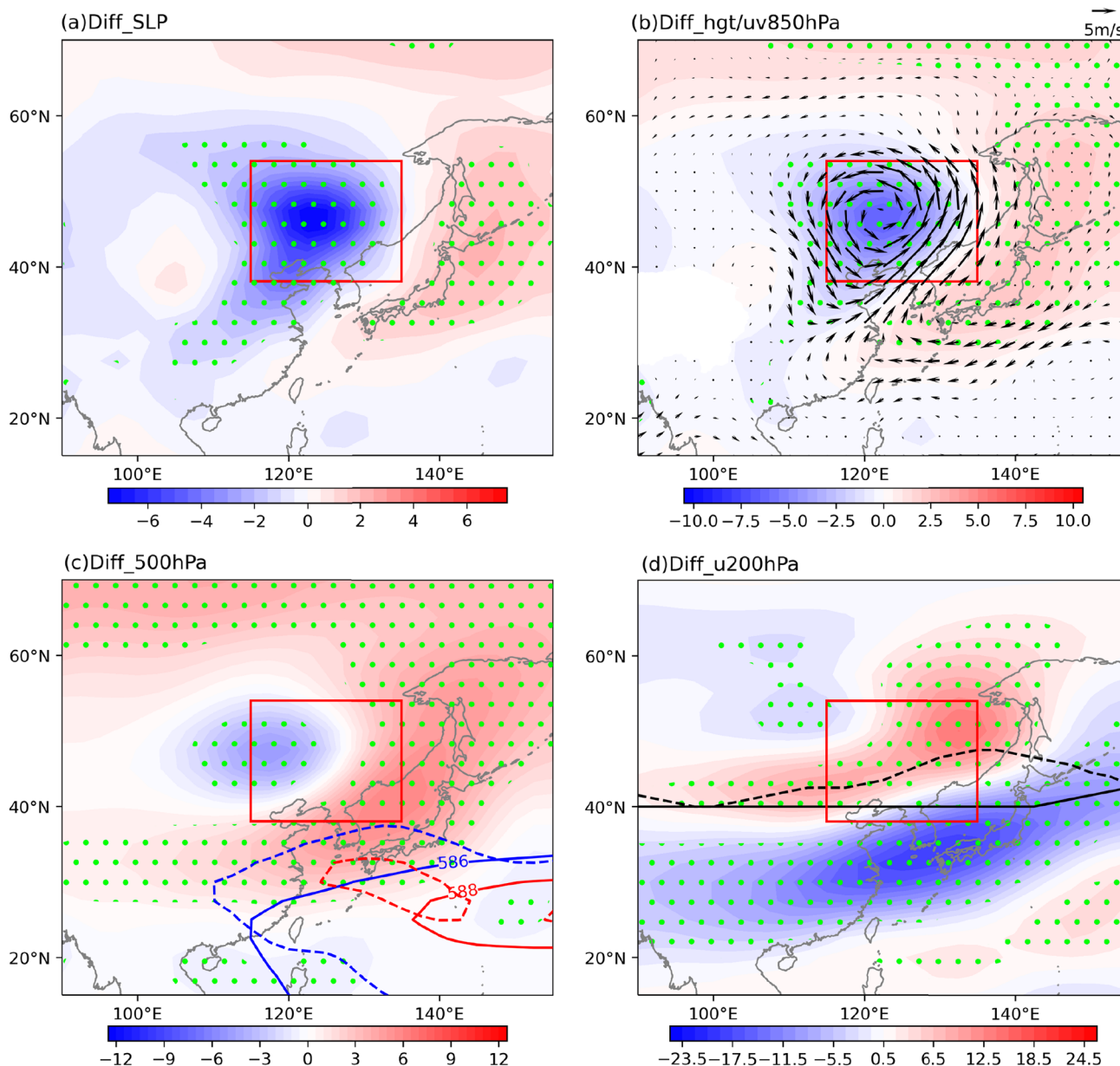
Fig. 4 Circulation anomalies associated with CHP events during summer: **a** sea level pressure (SLP, mb), **b** 850-hPa geopotential height (hPa, shadings) and horizontal wind (m s^{-1}, vectors), **c** 500-hPa geopotential height (hPa, shadings) with a 588-gpm (red lines) and a 586-gpm (blue lines) mean position in summer at 500 hPa (dashed lines are for CHP events and solid lines are the summer mean position during 1961–2020), and **d** 200-hPa zonal wind (m s^{-1}, shadings) and the jet axis (black lines). Stippling areas indicate values that significantly exceed the 95% confidence level, estimated using the Student's *t*-test. The red rectangle represents the NEC region

divergence appears over the Northwest Pacific and both southern and western China when CHP events occur. The intensified southerly flow over eastern China carries warm moist air from the Northwest Pacific and southern China northward across the southern boundary of NEC. Additionally, near the surface, the westerly flow from inland areas across the western boundary and the easterly flow from the mid-latitude western Pacific across the eastern boundary also contribute to the moisture convergence

anomalies over NEC. Hence, notable moisture convergence anomalies dominate NEC. At 850 hPa, the transport of moisture across the eastern boundary plays a negative role in the net moisture budget over NEC (Fig. 7b), which is different from the case of the near-surface transport (Fig. 7a). It can also be observed that anomalous southwesterly flow transports water vapor from the subtropical Northwest Pacific and southern China northward to NEC across the southern boundary, which is consistent with the
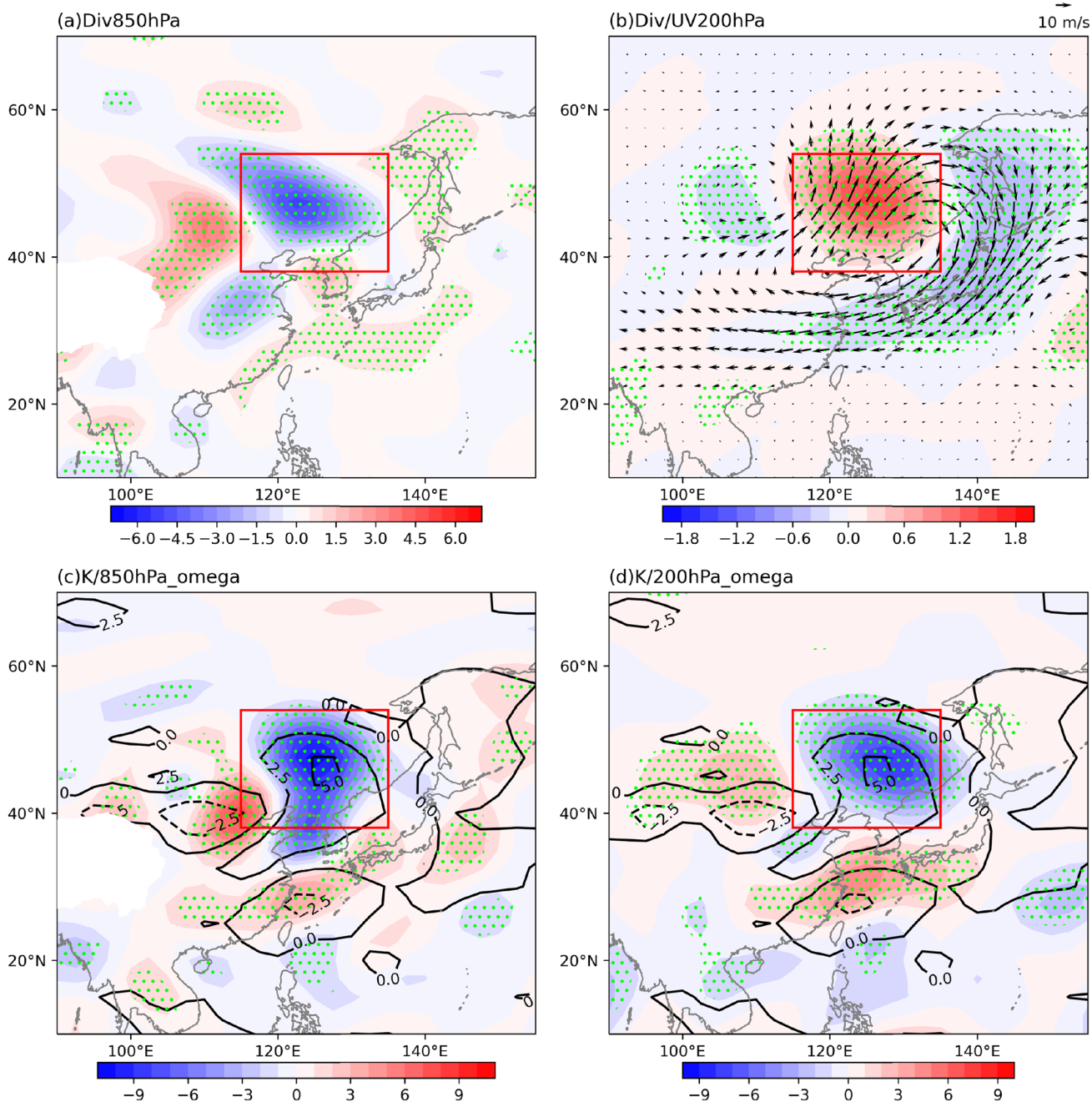
Fig. 5 Spatial distributions of **a** 850-hPa horizontal wind divergence anomalies (10^{-6} s^{-1}, shadings), **b** 200-hPa horizontal wind divergence anomalies (10^{-5} s^{-1}, shadings) and horizontal wind anomalies (m s^{-1}, vectors) between CHP events and the summer mean during 1961–2020, **c** same as **a** but for the K index (°C, contours) and 850- hPa vertical velocity (10^{-2} m s^{-1}, shadings), **d** same as **c** but for 200- hPa vertical velocity (10^{-2} m s^{-1}, shadings). Stippling areas indicate values that significantly exceed the 95% confidence level, estimated using the Student's t-test. The red rectangle represents the NEC region

near-surface transport. The northwesterly flow is enhanced in comparison with the climatology and it transports water vapor from inland areas eastward to NEC across the western boundary. Thus, remarkable moisture convergence anomalies affect NEC, although their magnitude is less than that near the surface. However, different anomalies are observed at middle and upper levels (Fig. 7c, d). The WVT at the northern and eastern boundaries plays a dominant but negative role in the net moisture budget over NEC in comparison with that in the lower troposphere. The WVT across the southern and western boundaries contributes only minimally to water vapor accumulation over
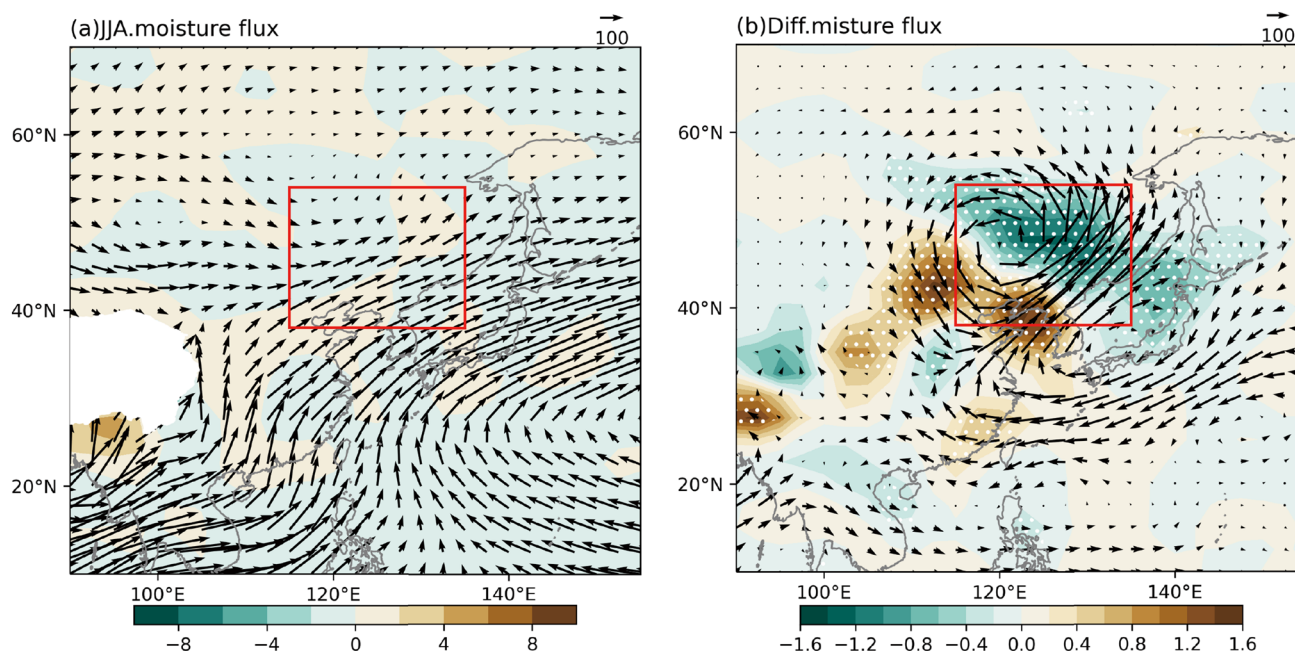
Fig. 6 a Climatology of vertically integrated moisture flux from the surface to 300 hPa (kg m^{-1} s^{-1}, vectors) and its divergence (10^{-4} kg m^{-2} s^{-1}, shadings) in summer during 1961–2020. **b** Spatial distributions of integrated water vapor transport (kg m^{-1} s^{-1}, vectors) and divergence of water vapor flux (10^{-4} kg m^{-2} s^{-1}, shadings) anomalies between the CHP events and the climatology during 1961–2020. Stippling areas indicate values that significantly exceed the 95% confidence level, estimated using the Student's *t*-test

NEC. Hence, anomalous moisture divergence is dominant over NEC at middle and upper levels.

We calculate the averaged WVT budget across each boundary during summer and for the CHP events during 1961–2020 (Table 2). Generally, the WVT across both southern and western boundaries of NEC contributes positively to water vapor accumulation over NEC, while the WVT across both northern and eastern boundaries makes a negative contribution. Climatologically, the net WVT budget is 12.00×10^7 kg s^{-1} across the southern boundary, -2.21×10^7 kg s^{-1} across the northern boundary, 13.58×10^7 kg s^{-1} across the western boundary, and -20.47×10^7 kg s^{-1} across the eastern boundary. Comparatively, when CHP events occur, the net influx is 32.6×10^7 kg s^{-1} across the southern boundary and 20.36×10^7 kg s^{-1} across the western boundary. The net outflux is 6.84×10^7 kg s^{-1} across the northern boundary and 31.02×10^7 kg s^{-1} across the eastern boundary. Hence, water vapor influx and outflux are both intensified remarkably during CHP events relative to the climatology. Specifically, the increment of net WVT influx across the southern (western) boundary of NEC for CHP events accounts approximately 171.67% (49.93%) to summer climatology. The summer net moisture budget is 2.90×10^7 kg s^{-1} at NEC for the climatology, and increases to 15.10×10^7 kg s^{-1} for CHP events. The increment of net moisture budget for CHP events accounts approximately 420.69% to the climatology.

Such an abundant supply of moisture is beneficial to the occurrence of CHP events over NEC.

Figure 8 shows the evolution of the areal mean precipitation, net WVT budget, and WVT budget across each boundary for 3 days before and 1 day after the occurrence of CHP events over NEC. The CHP is represented as time step 0, and the time steps of -1 and 1 indicate the day before and the day after a CHP event, respectively. The net moisture budget generally begins to increase 2 days before the CHP, peaks 1 day before the CHP (time step: -1), and then declines rapidly (Fig. 8a). Clearly, results from the moisture budget across the southern boundary are nearly the same as the net moisture budget (Fig. 8b). The net moisture influx across the southern boundary plays an important role on the day of occurrence of the CHP. It is notable that the net moisture budget of the southern boundary is mostly > 0 (i.e., net moisture influx) for the 3 days before the occurrence of the CHP, which implies that WVT across the southern boundary always contributes to the net moisture budget over NEC. Although weaker than that across the southern boundary, the moisture budget across the western boundary begins to accumulate 3 days before the CHP (Fig. 8d), and it contributes positively to the net moisture influx during the CHP event (Table 2). Moreover, the moisture budget across the northern boundary changes little from 3 days before the CHP to 1 day after the CHP (Fig. 8c). The net moisture outflux across the eastern boundary increases after time step -1 (Fig. 8e).
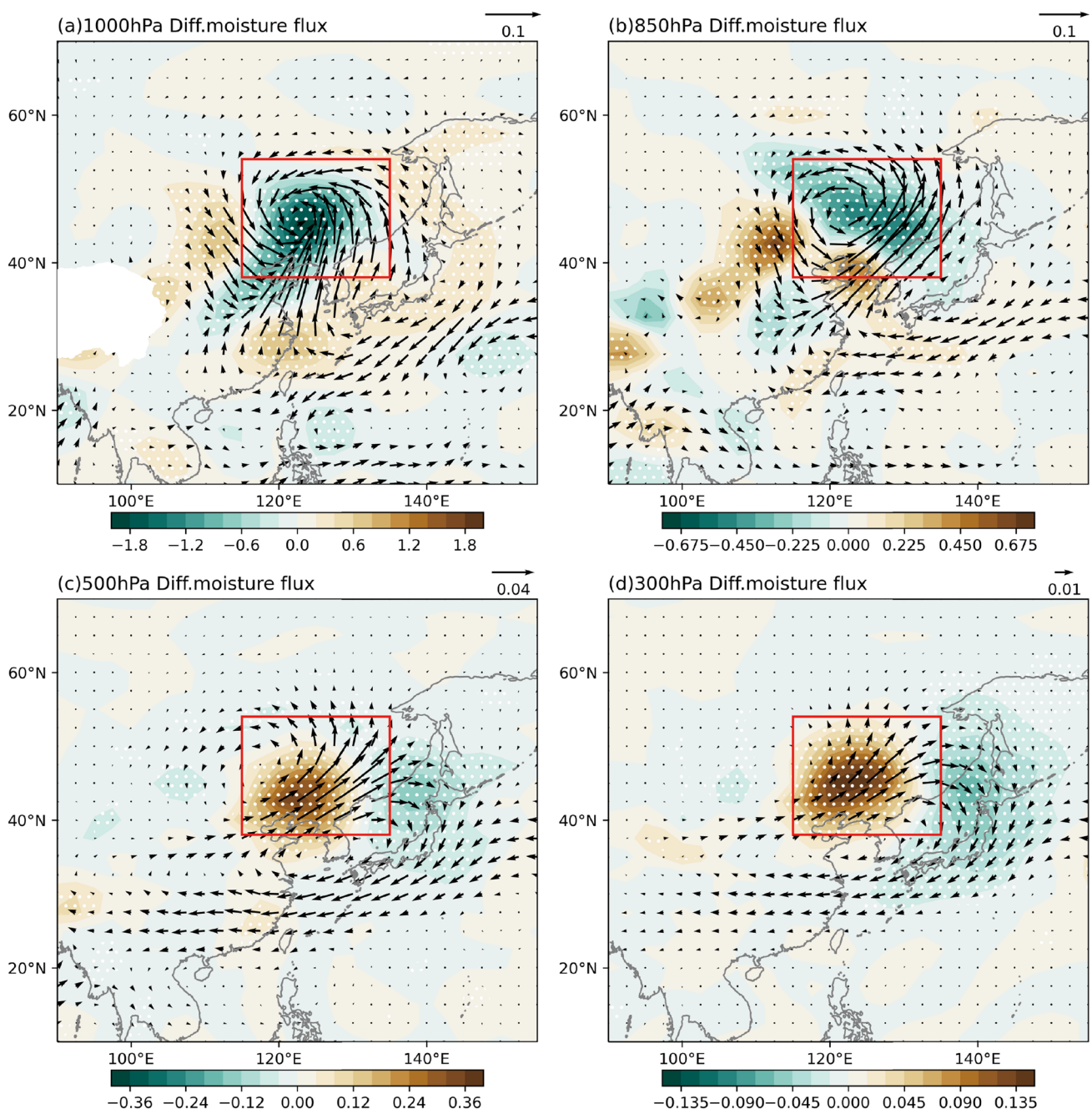
Fig. 7 Spatial distributions of water vapor transport (m s^{-1}, vectors) and divergence of water vapor flux (10^{-7} s^{-1}, shadings) anomalies between the CHP events and the climatology during 1961–2020: **a** 1000 hPa, **b** 850 hPa, **c** 500 hPa, and **d** 300 hPa. Stippling areas indicate values that significantly exceed the 95% confidence level, estimated using the Student's t-test

	WVT budget (10^7 kg s^{-1})	CHP	Summer	Difference	Ration (%) (difference/summer)
Table 2 Water vapor transport budget across each boundary of NEC for summer mean and CHP events during 1961–2020 (WVT budget units: 10^7 kg s^{-1})	Southern boundary	32.60	12.00	20.60	171.67
	Northern boundary	− 6.84	− 2.21	− 4.63	209.50
	Western boundary	20.36	13.58	6.78	49.93
	Eastern boundary	− 31.02	− 20.47	− 9.55	46.65
	Net flux	15.10	2.90	12.20	420.69
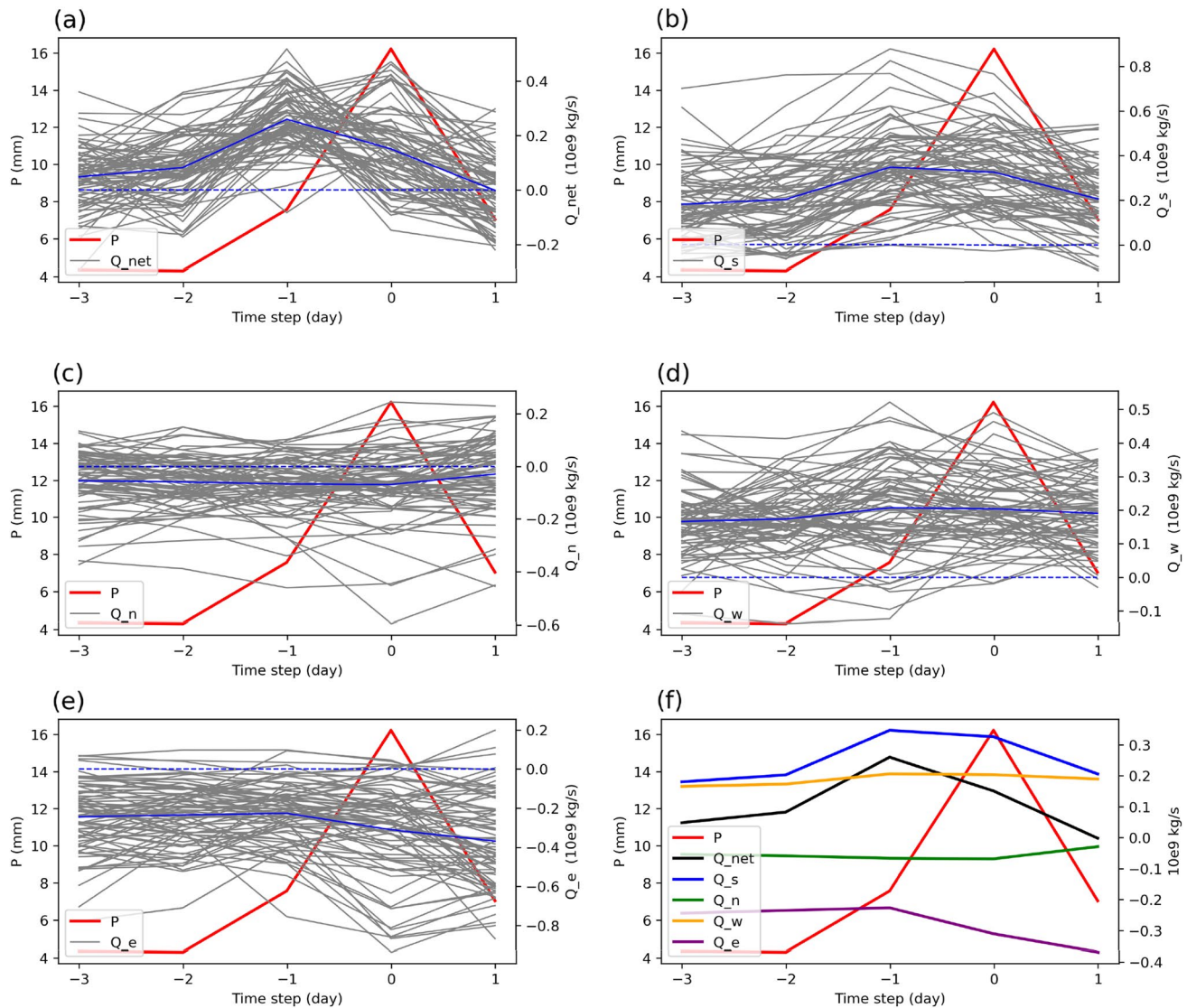
Fig. 8 Evolution of **a** the net budget (Q_net), the WVT budget across, **b** the southern (Q_s), **c** the northern (Q_n), **d** the western (Q_w), and **e** the eastern (Q_e) boundaries of NEC and the regionally averaged daily precipitation (P) in the 3 days before and 1 day after the CHP over NEC, **f** same as **a**, but showing the average evolution of WVT budget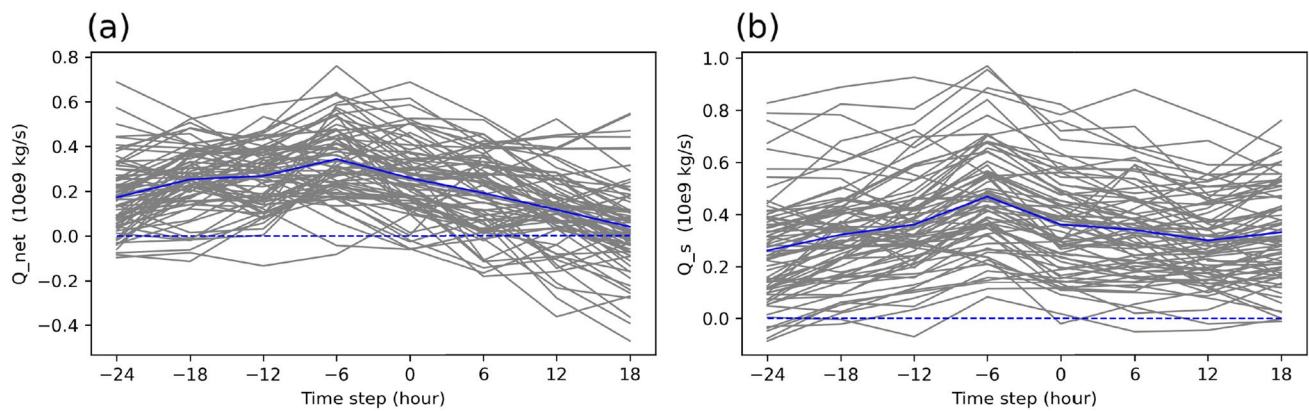 and precipitation of multiple cases. Time step 0 represents the start of the CHP. The gray lines represent the WVT budget of the 75 CHP cases, the blue solid lines represent their averages, the blue dashed lines represent zero values of the WVT budget, and red lines represent precipitation of multiple cases averages (WVT budget units: 10^9 kg s^{-1}, precipitation units: mm)

The above results show that WVT 1 day before a CHP event plays a key role in the water vapor accumulation over NEC.

Generally, the net moisture budget that begins to increase 2 days before the CHP and peaks 1 day before the CHP is predominantly attributed to the pre-accumulated net WVT influx across the southern boundary. The CHP is closely connected to the WVT budget at the southern boundary at time steps −1 and 0 with correlation coefficients of 0.41 and 0.40, respectively (significant at the 99% confidence level). This verifies that CHP depends not only on coinstantaneous WVT but also on pre-accumulated moisture influx across the southern boundary, which is in accord with the findings

of Sun et al. (2007) and Sun and Wang (2013). Thus, the details of the WVT budget across the southern boundary for 1 day before and 1 day after CHP events is discussed in the following.

The evolution of the net moisture budget and the moisture influx across the southern boundary for 24 h before and 18 h after CHP are shown in Fig. 9a, b, respectively. Further analyses show that both the net moisture budget and the moisture influx across the southern boundary increases consistently approximately 24 h before the CHP, peaks 6 h before the CHP, and then diminishes gradually, indicating that the phase of precipitation lags the phase of the net moisture

Fig. 9 Evolution of **a** the net WVT budget and **b** the WVT budget at the southern boundary in the 24 h before and 18 h after CHP in NEC. Time step 0 represents the time of the CHP, the gray lines represent the WVT budget of the 75 CHP cases, the blue solid lines represent their averages, and the blue dotted lines represent the zero values of the WVT budget (WVT budget units: 10^9 kg s^{-1})

budget by 6 h. This implies that the accumulation of water vapor 1 day earlier, especially the net moisture budget 6 h earlier, is of great importance for prediction of the occurrence of CHP events.

4 Conclusions

Based on the threshold method, this study defined CHP events over NEC and then explored the characteristics of CHP events, and the associated atmospheric circulation and moisture transportation anomalies. The main conclusions derived are summarized as follows.

The CHP events mainly occur during midsummer, especially in July. The numbers of CHP events during the latter 10 days of July significantly exceed those in other 10-day periods during the summer months. The frequency and the intensity of CHP events over NEC display significant interdecadal variation during the previous six decades, i.e., both decreased/weakened after the mid-1970s, increased/strengthened after the early 1980s, and decreased/weakened after the late 1990s. The occurrence of CHP events diminished during the 2000s and 2010s. In comparison with the climatology, CHP events are usually accompanied by marked negative height anomalies centered over NEC in the lower troposphere, westward and northward shifts of the WNPSH in the middle troposphere, and northward shift and intensification of the westerly jet in the upper troposphere. Additionally, significant lower-layer convergence anomalies and upper-layer divergence anomalies over NEC lead to increased atmospheric instability and upward movement in the vertical direction that play important roles in the occurrence of local CHP. The CHP events co-occur with strengthened water vapor transport, especially that in the lower troposphere. The net moisture budget begins to increase 2 days before the CHP and it peaks 1 day before the CHP. Further results indicate that the phase of the net moisture budget, especially the moisture influx across the southern boundary, leads the CHP by 6 h. Furthermore, to reduce the uncertainties from the different criterion to define the CHP, another two classifications (including 30% and 50% of the grid points over NEC) are calculated (Tables S3 and S5). Similar results can be obtained from these different cases (Tables S4 and S6, Figures S7–S24). It suggests that the results in this study are robust.

It should be mentioned that consistent atmospheric circulation anomalies and moisture transportation are observed when the strongest five CHP events appear, but with larger magnitude (Tables S1–S2, Figures S1–S6). The net moisture budget begins to increase 2 days before the occurrence of the strongest five CHP cases and peaks 6 h earlier. These results suggest that the moisture conditions 1 day earlier, especially 6 h earlier, are of predictive significance for the occurrence of CHP events over NEC.

Data availability The precipitation records can be obtained from CN05.1 dataset. The NCEP/NCAR reanalysis datasets can be downloaded from https://psl.noaa.gov/data/gridded/data.ncep.reanalysis.html.

Declarations

Conflict of interest The authors have not disclosed any competing interests.

References

Ban N, Schmidli J, Schär C (2015) Heavy precipitation in a changing climate: does short-term summer precipitation increase faster? Geophys Res Lett 42(4):1165–1172. https://doi.org/10.1002/2014GL062588

Breugem AJ, Wesseling JG, Oostindie K et al (2020) Meteorological aspects of heavy precipitation in relation to floods-an overview. Earth-Sci Rev 204:103171. https://doi.org/10.1016/j.earscirev.2020.103171

Cao F, Gao T, Dan L et al (2018) Contribution of large-scale circulation anomalies to variability of summer precipitation extremes in northeast China. Atmos Sci Lett 19(12):e867. https://doi.org/10.1002/asl.867

Chen HP, Sun JQ, Fan K (2012a) Decadal features of heavy rainfall events in EasternChina. Acta Meteorol Sin 26(3):289–303. https://doi.org/10.1007/s13351-012-0303-0

Chen HP, Sun JQ, Chen XL, Zhou W (2012b) CGCM projections of heavy rainfall events in China. Int J Climatol 32(3):441–450. https://doi.org/10.1002/joc.2278

Ding YH (1992) Summer monsoon rainfalls in China. J Meteor Soc Jpn 70(1B):373–396. https://doi.org/10.2151/jmsj1965.70.1b_373

Ding T, Chen LJ (2015) Circulation pattern for summer precipitation in northeast China and application of dynamical climate model information. Plateau Meteorol 34(4):1119–1130. https://doi.org/10.7522/j.issn.1000-0534.2014.00101 (**in Chinese**)

Du H, Wu Z, Zong S, Meng X, Wang L (2013) Assessing the characteristics of extreme precipitation over northeast China using the multifractal detrended fluctuation analysis. J Geophys Res Atmos 118(12):6165–6174. https://doi.org/10.1002/jgrd.50487

Fang YH, Chen HS, Teng FD, Wang XJ, Wang J, Zhao CY (2017) Changing contribution rate of heavy rainfall to the rainy season precipitation in Northeast China and its possible causes. Atmos Res 197:437–445. https://doi.org/10.1016/j.atmosres.2017.07.030

Gao J, Gao H (2018) Influence of the northeast cold vortex on flooding in Northeast China in summer 2013. J Meteor Res 32(2):172–180. https://doi.org/10.1007/s13351-018-7056-3

Gao Z, Hu ZZ, Zhu J et al (2014) Variability of summer rainfall in Northeast China and its connection with spring rainfall variability in the Huang-Huai region and Indian Ocean SST. J Clim 27(18):7086–7101. https://doi.org/10.1175/JCLI-D-14-00217.1

Gimeno L, Stohl A, Trigo RM et al (2012) Oceanic and terrestrial sources of continental precipitation. Rev Geophys 50(4):RG4003. https://doi.org/10.1029/2012RG000389

Gimeno L, Dominguez F, Nieto R et al (2016) Major mechanisms of atmospheric moisture transport and their role in extreme precipitation events. Annu Rev Environ Resour 41(1):117–141. https://doi.org/10.1146/annurev-environ-110615-085558

Gong Q, Wang HY, Wang PX (2006) Analysis of climate and anomaly features of summer precipitation in Northeast China. Meteor Sci Tech 34(4):387–393. https://doi.org/10.3969/j.issn.1671-6345.2006.04.007 (**in Chinese**)

Han T, Chen H, Wang H (2015) Recent changes in summer precipitation in northeast China and the background circulation. Int J Climatol 35(14):4210–4219. https://doi.org/10.1002/joc.4280

Han T, Wang H, Sun J (2017) Strengthened relationship between eastern ENSO and summer precipitation over northeastern China. J Clim 30(12):4497–4512. https://doi.org/10.1175/JCLI-D-16-0551.1

Han T, Wang H, Hao X et al (2019) Seasonal prediction of midsummer extreme precipitation days over Northeast China. J Appl Meteor Climatol 58(9):2033–2048. https://doi.org/10.1175/JAMC-D-18-0253.1

Hu KX, Lu RY, Wang DH (2010) Seasonal climatology of cut-off lows and associated precipitation patterns over Northeast China. Meteor Atmos Phys 106(1–2):37–48. https://doi.org/10.1007/s00703-009-0049-0

Hu P, Wang M, Yang L et al (2018) Water vapor transport related to the interdecadal shift of summer precipitation over northern East Asia in the late 1990s. J Meteor Res 32(5):781–793. https://doi.org/10.1007/s13351-018-8021-x

Huang RH, Liu Y, Feng T (2013) Interdecadal change of summer precipitation over eastern China around the late-1990s and associated circulation anomalies, internal dynamical causes. Chin Sci Bull 58(12):1339–1349. https://doi.org/10.1007/s11434-012-5545-9

Huang W, Feng S, Chen J et al (2015) Physical mechanisms of summer precipitation variations in the Tarim Basin in northwestern China. J Clim 28(9):3579–3591. https://doi.org/10.1175/JCLI-D-14-00395.1

IPCC (2021) Summary for policymakers. In: Masson-Delmotte V, Zhai P, Pirani A, Connors SL, Péan C, Berger S, Caud N, Chen Y, Goldfarb L, Gomis MI, Huang M, Leitzell K, Lonnoy E, Matthews JBR, Maycock TK, Waterfield T, Yelekçi O, Yu R, Zhou B (eds) Climate change 2021: the physical science basis. Contribution of working group I to the sixth assessment report of the intergovernmental panel on climate change. Cambridge University Press, Cambridge, pp 3−32. https://doi.org/10.1017/9781009157896.001

Kalnay E, Kanamitsu M, Kistler R et al (1996) The NCEP/NCAR 40-year reanalysis project. Bull Am Meteor Soc 77:437–472. https://doi.org/10.1175/1520-0477(1996)077%3c0437:tnyrp%3e2.0.co;2

Li F (2019) Analysis of extreme precipitation changes in northeast China in recent 52 years. Heilongjiang Hydraul Sci Technol 47(7):16–20. https://doi.org/10.14122/j.cnki.hskj.2019.07.004 (**in Chinese**)

Li H, Chen H, Wang H (2016) Changes in clustered extreme precipitation events in South China and associated atmospheric circulations. Int J Climatol 36(9):3226–3236. https://doi.org/10.1002/joc.4549

Li XR, Fan K, Xu ZQ (2019) Decrease in extreme precipitation in summer over east Northern China and the water-vapor transport characteristics after year 2000. Chin J Atmos Sci 43(5):1109–1124. https://doi.org/10.3878/j.issn.1006-9895.1902.18198 (**in Chinese**)

Liang L, Li L, Liu Q (2011) Precipitation variability in northeast China from 1961 to 2008. J Hydrol 404(1–2):67–76. https://doi.org/10.1016/j.jhydrol.2011.04.020

Lin YT, Zhao CY, Fang YH et al (2021) Analysis of spatiotemporal variation of precipitation and new characteristics of atmospheric circulation factors in early summer and midsummer in Northeast China. J Meteorol Environ 005:037. https://doi.org/10.3969/j.issn.1673-503X.2021.05.010 (**in Chinese**)

Meng X, Zhang Y, Gao SY, Xu LL, Shan LL, Fan XB (2022) Characteristics of midsummer precipitation in northeast china during

the last 60 years and its relationship with different types El Niño events. Water Soil Conserv Res 29:170–178. https://doi.org/10.13869/j.cnki.rswc.2022.02.006 (**in Chinese**)

Piao J, Chen W, Chen S (2021) Water vapour transport changes associated with the interdecadal decrease in the summer rainfall over Northeast Asia around the late-1990s. Int J Climatol 41(S1):1469–1482. https://doi.org/10.1002/joc.6780

Shen BZ, Lin ZD, Lu RY et al (2011) Circulation anomalies associated with interannual variation of early- and late-summer precipitation in Northeast China. Sci China Earth Sci 54(7):1095–1104. https://doi.org/10.1007/s11430-011-4173-6

Song S, Li L, Chen X, Bai J (2015) The dominant role of heavy precipitation in precipitation change despite opposite trends in west and east of northern China. Int J Climatol 35(14):4329–4336. https://doi.org/10.1002/joc.4290

Sun JQ, Ao J (2013) Changes in precipitation and extreme precipitation in a warming environment in China. Chin Sci Bull 58(12):1395–1401. https://doi.org/10.1007/s11434-012-5542-z

Sun B, Wang H (2013) Water vapor transport paths and accumulation during widespread snowfall events in Northeastern China. J Clim 26(13):4550–4566. https://doi.org/10.1175/jcli-d-12-00300.1

Sun L, Shen B, Gao Z et al (2007) The impacts of moisture transport of East Asian Monsoon on summer precipitation in Northeast China. Adv Atmos Sci 24(4):606–618. https://doi.org/10.1007/s00376-007-0606-8

Sun B, Zhu Y, Wang H (2011) The recent interdecadal and interannual variation of water vapor transport over eastern China. Adv Atmos Sci 28(5):1039–1048. https://doi.org/10.1007/s00376-010-0093-1

Trenberth KE, Smith L, Qian T et al (2007) Estimates of the global water budget and its annual cycle using observational and model data. J Hydrometeor 8(4):758–769. https://doi.org/10.1175/jhm600.1

Wang HJ, He SP (2015) The North China/Northeastern Asia severe summer drought in 2014. J Clim 28(17):6667–6681. https://doi.org/10.1175/JCLI-D-15-0202.1

Wang B, Wu R, Lau KM (2013) Changes in extreme precipitation over northeast China, 1960–2011. Quat Int 298:177–186. https://doi.org/10.1016/j.quaint.2013.01.025

Wang L, Wu Z, He H et al (2017) Changes in summer extreme precipitation in Northeast Asia and their relationships with the East Asian summer monsoon during 1961–2009. Int J Climatol 37(1):25–35. https://doi.org/10.1002/joc.4683

Wang R, Zhang J, Guo E et al (2019) Spatial and temporal variations of precipitation concentration and their relationships with large-scale atmospheric circulations across Northeast China. Atmos Res 222:62–73. https://doi.org/10.1016/j.atmosres.2019.02.008

Wu J, Gao XJ (2013) A gridded daily observation dataset over China region and comparison with the other datasets. Chin J Geophys 56(4):1102–1111. https://doi.org/10.6038/cjg20130406 (**in Chinese**)

Wu Y, Ji H, Wen J et al (2019) The characteristics of regional heavy precipitation events over eastern monsoon China during 1960–2013. Glob Planet Change 172:414–427. https://doi.org/10.1016/j.gloplacha.2018.11.001

Wu X, Meng F, Liu P et al (2021) Contribution of the northeast cold vortex index and multiscale synergistic indices to extreme precipitation over Northeast China. Earth Sp Sci 8(1):e2020EA001435. https://doi.org/10.1029/2020EA001435

Xu JA, Li XH (2021) Spatiotemporal evolution characteristics of extreme precipitation events in northeastern China in recent 50 years. Clim Change Res Lett 10:352–364. https://doi.org/10.12677/CCRL.2021.104041 (**in Chinese**)

Xu X, Du Y, Tang J, Wang Y (2011) Variations of temperature and precipitation extremes in recent two decades over China. Atmos Res 101:143–154. https://doi.org/10.1016/j.atmosres.2011.02.003

Xu ZQ, Fan K, Wang HJ (2015) Decadal variation of summer precipitation over China and associated atmospheric circulation after the late 1990s. J Clim 28(10):4086–4106. https://doi.org/10.1175/jcli-d-14-00464.1

Yao C, Qian W, Yang S et al (2010) Regional features of precipitation over Asia and summer extreme precipitation over Southeast Asia and their associations with atmospheric-oceanic conditions. Meteorol Atmos Phys 106(1–2):57–73. https://doi.org/10.1007/s00703-009-0052-5

Yu X, Ma Y (2022) Spatial and temporal analysis of extreme climate events over Northeast China. Atmosphere 13(18):1197. https://doi.org/10.3390/atmos13081197

Zhang S, Chen Y, Luo Y, Liu B, Ren G, Zhou T et al (2022) Revealing the circulation pattern most conducive to precipitation extremes in Henan Province of North China. Geophys Res Lett 49:e2022GL098034. https://doi.org/10.1029/2022GL098034

Zhao S, Sun J (2006) Study on cut-off low-pressure systems with floods over Northeast Asia. Meteorol Atmos Phys 96:159–180. https://doi.org/10.1007/s00703-006-0226-3

Zhao J, Zhou J, Yang L et al (2018) Inter-annual and inter-decadal variability of early-and late-summer precipitation over northeast China and their background circulation. Int J Climatol 38(6):2880–2888. https://doi.org/10.1002/joc.5470

Zhou TJ, Yu RC (2005) Atmospheric water vapor transport associated with typical anomalous summer rainfall patterns in China. J Geophys Res. https://doi.org/10.1029/2004JD005413

Zhu QG (2007) Principle of synoptic meteorology. China Meteorological Press, Beijing, p 344 (**in Chinese**)

Publisher's Note Springer Nature remains neutral with regard to jurisdictional claims in published maps and institutional affiliations.